AIAA JOURNAL
Vol. 42, No. 11, November 2004

Comparative Study of Different Pressure-Sensitive-Paint Image Registration Techniques

L. Venkatakrishnan*
National Aerospace Laboratories, Bangalore 560 017, India

Image alignment plays an important role in pressure-sensitive-paint (PSP) data processing. A systematic comparative study of two commonly used approaches, namely, image transformation using image-warping transforms before ratioing and, alternatively, image mapping on to three-dimensional model space (using resection methodology prior to ratioing) prior to ratioing, is attempted here. PSP results along with conventional static port data as on a generic aircraft model at a freestream Mach number of 0.6 and incidence of 10 deg (taken from earlier work) are utilized to critically assess the merit of the preceding two approaches. The analyses show that image-warping methods can result in larger errors in regions of strong spatial gradients of pressure and on bodies that are significantly three dimensional. Further, the resolution obtained from the resection approach is significantly greater (of the order of less than a pixel) compared to the transform methods.

Nomenclature

a_n, b_n, A, B, C, D	=	transform coefficients
C_p	=	model surface-pressure coefficient
f	=	focal length of camera lens
I	=	image to be warped on to base image
I_0	=	base image onto which other images are warped
L_n	=	direct linear transform coefficients
X, Y, Z	=	point in model space
X_c, Y_c, Z_c	=	camera perspective center
(x, y)	=	point on base image
(x', y')	=	point on image to be warped
ω, ϕ, κ	=	Euler angles

I. Introduction

THE technique of pressure-sensitive paints (PSP) for measurement of surface-pressure distributions on wind-tunnel models has gained increasing acceptance in recent years, as a tool for both industry and research.[1] The method uses a PSP coated on a model, digital imaging using a charge-coupled-device (CCD) camera and image processing to obtain surface-pressure information with a fair degree of resolution. The approach can be of either the luminescent lifetime or luminescent intensity type. The lifetime pressure is not dependent on illumination intensity, and hence the paint has a single pressure-sensitive luminophore. The intensity method uses either a unary (pressure-sensitive molecule) or binary luminophore (both intensity and pressure-sensitive molecules). The binary paint provides a means to normalize the pressure-sensitive image by the illumination sensitive image and thus eliminate the effects of spatial and temporal nonuniformity in illumination, coating thickness and luminophore concentration. The intensity-based method requires a ratio between normalized wind-on and wind-off conditions. The wind-off condition is also termed the reference and typically taken to be ambient values. The images are captured using scientific grade cooled CCD digital cameras, which exhibit good linearity and have high-intensity resolution (12 to 16 bits) and physical resolution (up to 2048×2048 pixels).

Received 12 December 2003; revision received 1 June 2004; accepted for publication 14 June 2004.

*Scientist, Experimental Aerodynamics Division. Member AIAA.

The various steps in PSP data processing include 1) calibration of the paint and converting image intensities to pressure; 2) application of corrections for nonideal imaging, which include alignment, correction for optical distortions etc.[1]; and 3) determining and applying a transformation from image to model coordinates. The second step for most PSP methods using binary paint involves a ratio-of-ratios between a reference (wind-off) image and a pressure (wind-on) image, each of which are normalized by the illumination to compensate for spatial and temporal variation in light intensity. The images are ratioed after an alignment process termed registration. The errors in image alignment arise mainly from the following two factors: first, that the model might not be in exactly the same position between the wind-on and wind-off images; and second, the two views of the model, one from each camera (e.g., for a binary paint), are generally different. The image alignment errors coupled with the ratioing process could result in certain inaccuracy in the PSP data. The third step is the mapping of image coordinates on the three-dimensional model using photogrammetric techniques in a method termed resection.[2,3] The term "resection" in photogrammetry is strictly defined as determination of the exterior orientation parameters of a camera for given internal orientation parameters. However, in the PSP community this has loosely come to mean the mapping onto a surface grid after the camera parameters are known, which involves alignment of the images with each other prior to normalization and ratioing.

It has long been recognized[1,4,5] that the accuracy of a PSP system depends on many factors among which image alignment[2–8] and temperature[1,4] are the most important. In this paper, we will address only the issues relating to image alignment in the context of a binary paint. Unless otherwise mentioned, "paint" refers to binary paint. There are two very commonly used methods to obtain the ratio-of-ratios. The first, more commonly used, is to use some form of image transformation method to warp all the images on to the base image followed by ratioing, and thereafter map the ratio on to the surface grid of the model using resection. The alternative is to form the ratios in model rather than image coordinates by first individually resecting all images onto the model grid. The image-warping approach, more commonly used in PSP work, seems suitable and adequate when the model surface is largely flat (with minimum transverse curvature) and model deflections and deformations are small between wind-off and wind-on images. However, more accurate results can be obtained by resection prior to ratioing, particularly for three-dimensional models in general and with model deflections between wind off and wind on; simple image-warping techniques are not sufficient,[7,9] and the error can be significant as we shall see in succeeding sections.

A third (less explored) approach is to use correlation-based image registration methods. In this approach, local displacement vectors

are found from cross-correlating interrogation windows between the wind-off and wind-on cases. Weaver et al.[10] proposed a quantum pixel energy distribution algorithm that uses spatial anomalies as markers and then used a pixel matching algorithm, which, although it eliminates markers, is extremely time consuming, and Park and Sung[11] used a layer of diffuse markers by spraying gray paint coarsely over the base coat. However, the effect on calibrated pressure sensitivity has not been studied.

Photogrammetric techniques, although not in general widespread use in wind-tunnel testing practice, have been used recently for luminescent paints and model deformation methods. Donovan et al.,[12] LeSant and Merienne,[9] Bell and McLachlan,[3] Samtaney,[13] and Liu et al.[7] have described the application of these methods to PSP data processing. For example, Donovan et al.[12] and Bell and McLachlan[3] use a two-step method, first warping all images onto a base (wind-off) image, ratioing, and then applying the resection method to map the final ratio-of-ratios (herein after referred to as field image) obtained from image warping to the model grid rather than individual resection prior to ratioing. However, the effects of (imaging) lens distortion have been only approximately accounted for in their analysis. LeSant and Merienne,[9] Samtaney,[13] Liu et al.,[7] and Fonov et al.[14] point out that more accurate results are obtained by adopting the second approach just outlined, namely, individual resectioning of all images prior to ratioing. Liu et al.[7] have proposed an optimization method for estimating the effects of image distortion introduced by the camera optics wherein the distortion can be estimated from a single image. Ruyten[15] used photogrammetric principles to create a mathematical model for measuring position, attitude, and deformation using multiple cameras in a wind tunnel. Ruyten and Sellers[16] compared processing schemes and showed that the time for PSP data reduction could be limited to less than 10 s by usage of parallel processing schemes.

As just seen, although resection approaches has been discussed in earlier work, no systematic comparison of accuracies obtainable from the two major approaches, namely, image warping and resection, against conventional pressure port data has been published so far. This analysis is carried out using the PSP results obtained on a generic wing-body model for a binary paint. The advantages and limitations of both image warping and resection prior to ratioing approaches are discussed, and their accuracies compared with pressure port data.

II. Image-Warping Methods

These methods are suited mainly for rigid-body motion of two-dimensional objects with small deformations, while being reasonably good approximations for small motions of three-dimensional objects. The geometry of the model, amount of deformation, number of markers, accuracy required, and computational resources determine the method chosen. Bell and McLachlan[3] have shown that the accuracy with which image registration much be performed is dependent on the maximum intensity gradient in the images and level of error that can be tolerated in the pressure measurement. They show that for a typical aircraft model (North American XB-70A) at a freestream Mach number of $M = 0.4$ with large pressure gradients ($\alpha = 15$ deg), a misregistration of 0.1 pixel widths would result in a C_p error of 0.1, which is quite significant. The accuracy requirement varies with flow condition and spatial location.

Six different transforms will be discussed; each of these transforms is best suited to a particular kind of distortion and deformation, which is both model geometry and flow dependent[4] and can be appropriately chosen by the user. Their description and applicability are detailed in the following subsections.

Prior to the transformation, corresponding features or control points or markers have to be located in the two images. The coefficients of the transform are then obtained by requiring that the transform match up corresponding control points. This leads to a set of linear algebraic equations, which is solved for the coefficients. Because each control point provides two coefficients, the minimum requirement of control points is half the number of coefficients required for the transformation. However, rather than rely on the presence of identifiable features in the image, it is common practice to place artificial markers in the form of black dots on the model for this purpose. If there are more points than necessary and the system is overdetermined, the equations are solved in a least-squares sense.

The markers are identified here by a manual process outlined in Sec. IV. Le Sant et al.[6] enumerate many fast and automatic algorithms for locating markers and establishing the correspondence of targets in wind-on and wind-off images. However, they point out that most of these algorithms are not always successful, leading to missed markers. Bell et al.[1] show that an error in locating a single marker point can have a overall effect on the transformed image, because of the global effect of the transforms used.

This paper will not go into the methods of marker location and identification, but will confine itself to the image registration techniques.

A. Projective Transform

This transform is most suitable when there is model deflection (between wind-off and wind-on cases) without any deformation and needs a minimum of four pairs of control points. This implies that this method must be chosen when the image appears "tilted," that is, straight lines remain straight, but parallel lines converge towards "vanishing points," which might or might not fall in the image. Given an wind-on image I to be mapped on to a base image I_0 (typically chosen as the wind-off reference image), any point (x, y) in I_0 is related to the corresponding point (x', y') in I by[17]

$$x = \frac{a_1 x' + a_2 y' + a_3}{c_2 x' + c_2 y' + 1}, \qquad y = \frac{b_1 x' + b_2 y' + b_3}{c_2 x' + c_2 y' + 1} \tag{1}$$

where $a_1, a_2, a_3, b_1, b_2, b_3, c_1, c_2$ are the transform coefficients.

B. Affine Transform

The affine transform needs just three pairs of control points. This is chosen when the image shape exhibits shearing type of deformation. Straight lines remain straight, parallel lines remain parallel, but rectangles become parallelograms. In general,[18]

$$\begin{vmatrix} x \\ y \end{vmatrix} = A \times \begin{vmatrix} x' \\ y' \end{vmatrix} + B \tag{2}$$

where

$$A = \begin{vmatrix} \cos(\theta) & -\sin(\theta) \\ \sin(\theta) & \cos(\theta) \end{vmatrix}, \qquad B = \begin{vmatrix} 0 \\ 0 \end{vmatrix}$$

for pure rotation and

$$A = \begin{vmatrix} 1 & 0 \\ 0 & 1 \end{vmatrix}, \qquad B = \begin{vmatrix} b_1 \\ b_2 \end{vmatrix}$$

for pure translation.

C. Linear Conformal

This transform is suited for cases where the image undergoes a combination of translation, rotation, and scaling, but the basic shape remains unchanged. In general,[19]

$$x' = A + Cx + Dy, \qquad y' = B - Dx + Cy \tag{3}$$

where $C = [\text{scale factor}] \times \text{cosine}([\text{angle of rotation}])$, $D = [\text{scale factor}] \times \text{sine}([\text{rotation angle}])$, and A and B are offsets for the center of rotation in output coordinates (translation).

The minimum number of marker pairs required for this transformation is just two; however, this transform does not yield good results unless the model is a very basic geometric shape and undergoes no deformation.

D. Polynomial Transform

Polynomial transformations are commonly used as the higher-order polynomials can account for nonlinear local deformation combined with model movement.[3] However, with increasing order the accuracy is limited because of to the inherent unstable nature of such polynomials. A first-order transformation requires only three targets, but second- and third-order polynomial transforms need a minimum of 6 and 10 targets, respectively. This takes the form of a polynomial series expansion[3]:

$$x = a_{00} + a_{10}x' + a_{11}y' + a_{20}x'^2 + a_{21}y'^2 + a_{23}x'y' + \dots$$

$$y = b_{00} + b_{10}x' + b_{11}y' + b_{20}x'^2 + b_{21}y'^2 + b_{23}x'y' + \dots \quad (4)$$

E. Piecewise Linear

This transform is based on Delaunay triangulation.[20] In this technique, each image is divided into triangles whose vertices are at chosen markers in the image. The location of any point in the wind-on image can be defined in terms of parametric coordinates in to the corresponding triangle in the wind-off image. This technique was first adapted for PSP image registration by Shanmugasundaram and Samareh-Abolhossani.[21] Although this is an accurate fit even when model distortion is nonuniform, it performs poorly when the model motion is nonlinear. This is because it is a piecewise linear fit, and as the individual triangles grow larger it will less accurately represent a surface that is fundamentally nonlinear. This technique needs a minimum of four pairs of marker, but accuracy improves considerably as the number of pairs are increased to 14[3].

F. Local Weighted Mean

In this technique, the local information is used with user-defined weighting at each point. The method[22] creates a mapping, by inferring a polynomial at each control point using neighboring control points. The mapping at any location depends on a weighted average of these polynomials.

For each control point in the base (wind-off) image, the N closest control points are found. Using these N points and their corresponding points in the input (wind-on) image, a second-order polynomial is inferred. The radius of influence of this polynomial is the distance, from the center control point to the farthest point used to infer the polynomial (using points in the wind-off image). The number of points used to define each polynomial can be set; hence, the radius of influence extends out to the farthest control point used to infer that polynomial. This is highly useful when the distortion varies locally and the piecewise linear method is not sufficient. Although a minimum of six pairs is required, small (<10) numbers of pairs can lead to ill-conditioned polynomials.[22]

III. Resection onto a Surface Grid

The transformation from model space coordinates (X, Y, Z) to image plane coordinates (x, y) is required in order to be able to determine the surface pressure at a physical point of interest in the model. This is termed as resection of an image onto the model surface grid.

A. Surface Grid

Figure 1 shows the body-fitted surface grid for the model used, generated using the GRIDGEN® software from Pointwise, Inc. Although only a representative grid has been shown in the figure for clarity, the multiblock grid used had a physical resolution of 2.5 mm in the streamwise and 1.3 mm in the spanwise direction, respectively. The grid was mirrored, with the mirror axis plane being the XY plane and composed of 12 blocks (or zones) with a total of 111,880 points. Figure 1 shows the number of points for zones one side of the mirror axis.

The availability of an accurate three-dimensional model for the surface grid is an important requirement, which is difficult to achieve when the model deforms under air loads. The resection approach outlined here is applicable to perfectly rigid models. Although model deformation could be a source of error and needs to be taken care of in the resection process, it is extremely difficult to characterize the actual model deformation under aerodynamic loads in a wind tunnel without actual measurements.

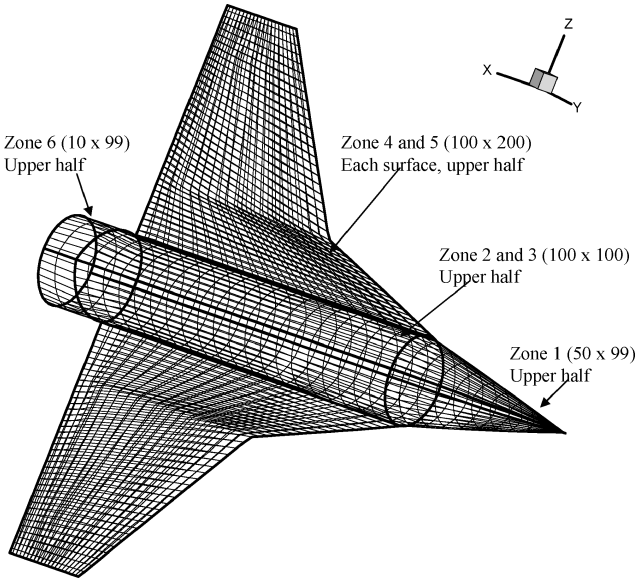

Fig. 1 Surface grid on model.

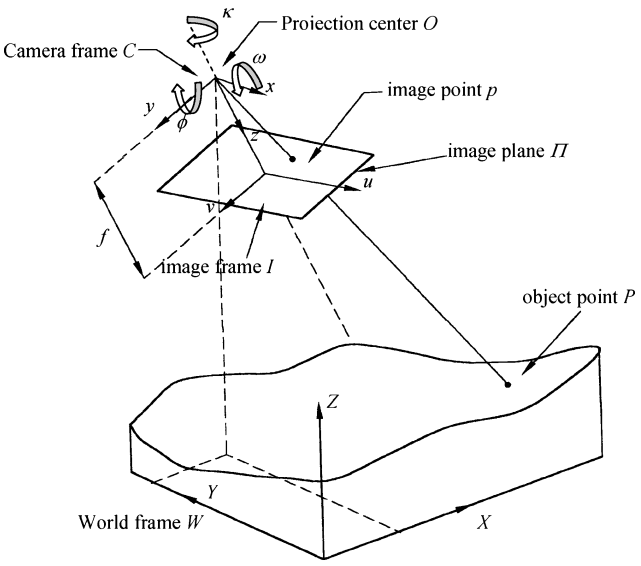

Fig. 2 Pinhole camera model.[23]

B. Camera Model

We first need to obtain a camera model, based on perspective projection, which, though nonlinear as opposed to the linear orthographic projection, provides an idealized mathematical framework and is quite accurate for high-quality camera systems. The camera model incorporating lens distortion proposed by Heikkilä[23] is used here along with his three-step approach. (Details of this model and the method of solution given by Samtaney[13] are given for reference in the Appendix.) Figure 2 shows a pure perspective projection (pinhole camera) camera model.[23] The lens of the camera is modeled by a single point called perspective center (X_c, Y_c, Z_c), which is also the origin of the image coordinate system (center of projection O) in model coordinate space. The camera model uses six exterior and eight internal parameters. The lens distortion terms can be modeled as the sum of radial distortion and decentering distortion as outlined by Slama.[24] The first step involves an initial guess for the camera exterior parameters (camera location and orientation), which are obtained either by the direct linear transform method[25] or by using the

nominal values of the focal length and image plane (CCD) size. The second step estimates the parameters of the forward camera model (which are intrinsic to the camera) by minimizing the weighted sum of squared differences between the observations and the model. The Levenberg–Marquardt method is then used for the optimization problem. Although this optimization approach necessitates the use of more than one image in order to obtain the observation error statistics, it results in very few (typically <50) iterations to reach the minimum as a result of the sophistication of the method. Liu et al.[7] use a sequential golden section search, which uses just a single image but does not work well for two-dimensional objects. Further, in this step, bias correction for circular control points is used. This is necessary because the usual assumptions of unbiased observations, identically distributed random noise in the image coordinate observations, and an ideal camera model for the mapping between the three-dimensional object and its image do not necessarily hold well. The third step is a nonrecursive step for reversing the distortion model for backward projection from the image plane (see Appendix for details).

IV. Experimental Data Utilized for the Assessment of Different Image Registration Methods

Experimental PSP data obtained on a generic aircraft wing-body configuration[26,27] in the 1.2-m trisonic wind tunnel at National Aerospace Laboratories are used to assess the accuracy of the different approaches and methods.

The model, having a span of 400 mm and a length of 430 mm, was coated with Optrod B1 binary paint (Fig. 3a). The lee side of the model was instrumented with 12 static pressure ports along the span (at a streamwise station of 344 mm from the nose) and four Cr-Al thermocouples on the model surface for the measurement of surface temperature during a blowdown. The PSP tests were made at freestream Mach numbers of 0.6 and 0.8 and at model incidence of 6 and 10 deg.

To perform the transformation, 32 markers (Fig. 3a) were provided on the model. The pressure ports were not used as markers. The imaging area of the model was slightly restricted (wing tip area cut off on one side) in order to maximize CCD resolution, and so only 30 of these markers were used. The physical locations of these markers were determined to an accuracy of 0.1 mm by using a three-axis coordinate measuring machine.

The paint emission data were acquired by two air-cooled scientific grade 12-bit CCD slow scan cameras (Model Sensicam SVGA) with resolution of 1280×1024 pixels. The sensor size was 16.9 mm (2/3 in.) and pixel size 6.7×6.7 μm. The schematic of the setup detailing camera locations and dimensions is shown in Fig. 3b.

The image coordinates of the marker centroids was found manually. This involved prescribing an 8×8 pixel square around the marker, and then an optimal intensity threshold using the histogram of this image area detected the marker area in the square. Thereafter, the extended-minima transform of the image is computed using the optimal threshold found. This returns a binary matrix, from which all of the connected pixels (marker) in it are found and the centroid computed. The error in determining centroid is <0.1 pixel.

To compare the accuracies of the different image registration methods, we utilize here only one test case, namely, PSP results at $M = 0.6$ and $\alpha = 10$ deg. The pressure is obtained from the intensity by use of a calibration function obtained by a priori calibration of the paint on a coupon. PSPs are temperature dependent. The temperature sensitivity of the Optrod B1 is about $\sim$0.35%/°C. Because the measurements were made in a blowdown wind tunnel,[27] there was a drop of a few degrees in model surface temperature during a blowdown. The experimental test case used here (see Ref. 23 for details) involved only a 2–3-deg drop in model temperature, and the spatial nonuniformity on the wing was within ± 1.5°C . Channa Raju and Viswanath[27] have suggested a temperature correction to PSP results based on the mean temperature of the model during PSP data acquisition. This methodology is used here as well; more details on the experiments and validation are available in Channa Raju and Viswanath.[27] The model mean temperature was 22°C for the test case analyzed.

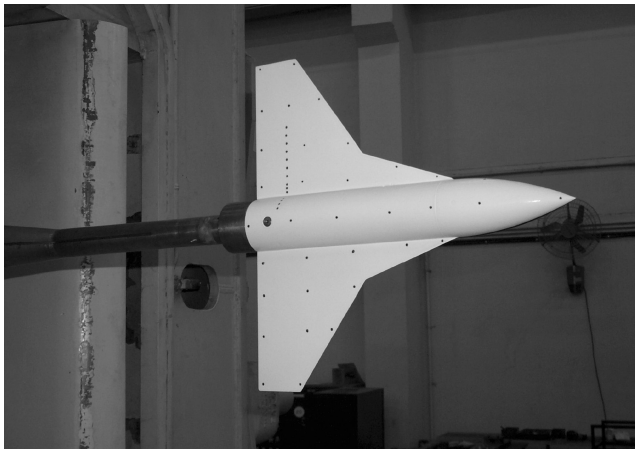

a) Aircraft wing-body model coated with Optrod-B1 paint

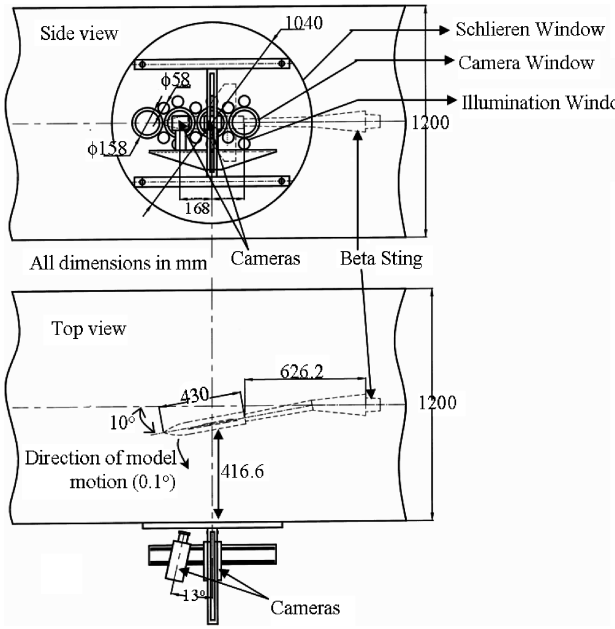

b) Schematic of measurement setup

Fig. 3 Experimental setup for PSP tests.[27]

V. Results and Discussion

A. Transformation Errors Using Image Warping

Figure 4, which is a ratio-of-ratios, shows the misalignment when no registration is performed. The four markers sets are clustered as groups of two, and the difference between the wind-off and wind-on condition is very small (very few pixels) compared to the difference (approximately 43 pixels) caused by the two camera perspectives. This followed from the fact that the experimental model utilized in the test case was fabricated from high-strength steel (EN-24) and had a wing thickness of 12 mm except in the vicinity of the beveled edges. Engineering estimates have shown that for the loads experienced by the model (freestream dynamic pressure 32,230 Pa for test conditions) the deflection is <0.1 deg, which is extremely small. It is very likely that the model deformation is negligible in this case. The misalignment of markers therefore is largely caused by differing camera perspective.

Figures 5a–5f show the field image obtained by using the different image-warping methods along with the maximum and average errors in each ratio. For each transformation the minimum number of markers needed was used, and the error computed from the rest. The centroids of these markers were determined in the same way as described in Sec. IV. Although it is common practice to filter out the markers prior to ratioing, here marker removal has not been effected in order to demonstrate the magnitude and spatial distribution of the error in transformation. We see that the clusters of markers

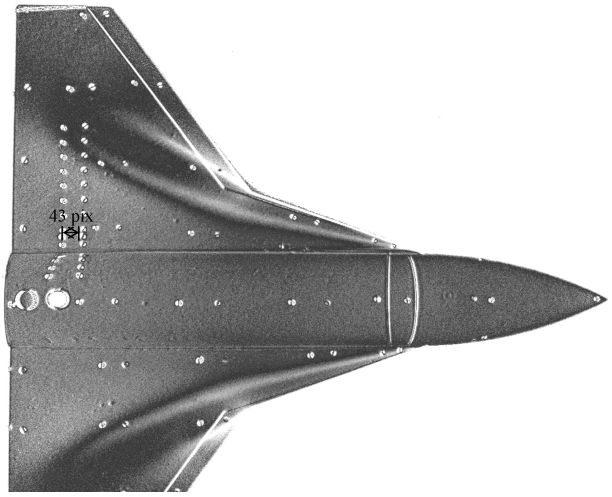

Fig. 4 Superimposed images showing marker misalignment when no registration is performed.

are closely spaced on the flat areas of the model, but spread out on the curved surface of the fuselage, showing that the maximum errors are always on the fuselage curved surface, for reasons discussed in Sec. I and by other studies.[7,9]

The maximum error (approximately 35 pixels) is observed for the affine and linear conformal methods. Although these two methods require only two and three pairs of markers respectively, they have the constraints of being suitable only for shearing deformation (affine) and simple geometric shape (linear conformal). Similarly, the error decreases to 22, 18, and 12 for the projective, polynomial (order 3), and local weighted mean methods, respectively. Thus, with increasing number of spatially distributed marker pairs used by a method, the error decreases correspondingly. This implies that for a complex geometry, which is not the simple combination of basic geometric shapes, methodologies that assume straight lines and simple shearing or combination of deflection and rotational movements are insufficient. The maximum error on the wings, which are flat two-dimensional bodies, is less than five pixels for all cases, which confirms the preceding conclusion.

The piecewise linear method that divides a surface into triangles for better representation of a fundamentally nonlinear surface thus

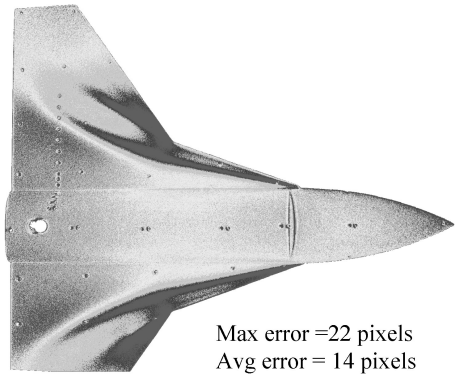

a) Projective

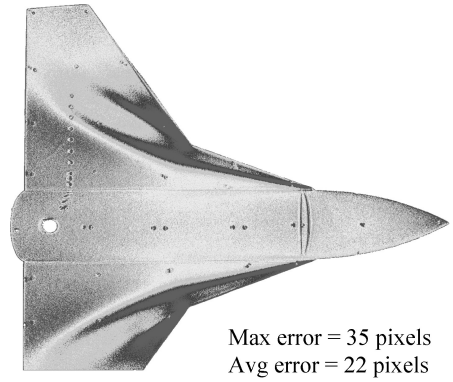

b) Affine

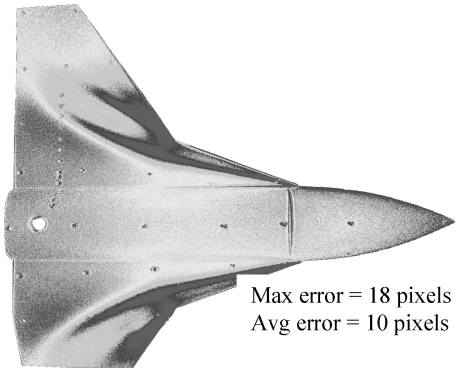

c) Polynomial (order 3)

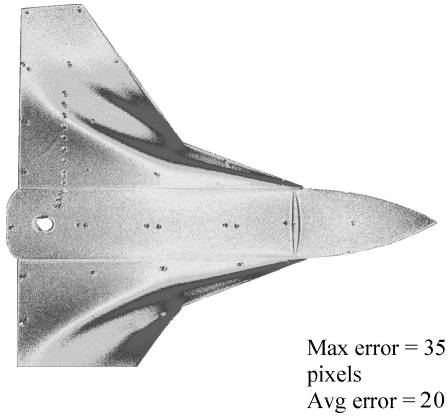

d) Linear conformal

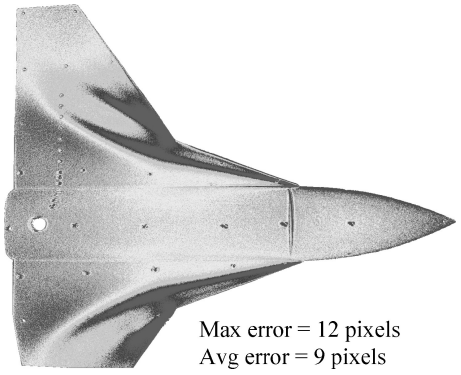

e) Local weighted mean

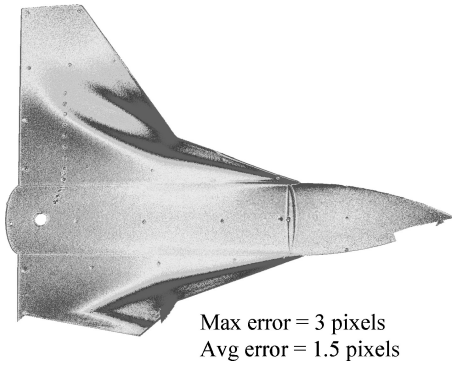

f) Piecewise linear

Fig. 5 Field image obtained through different transformation methods.

performs better with an error of only three pixels, as seen in Fig. 5f. However, the piecewise linear method performs very poorly where there are inadequate markers (e.g., near the peripheries), and the size of the triangle for mapping has to increase. This is in line with the observations of Bell and McLachlan.[3] Hence a third-order polynomial has been chosen for comparison of the image-warping approach to the resection approach,

B. Comparison of Results on the Surface Grid

The resection-before-ratio approach is used to directly obtain C_p on the grid using the camera model outlined in Sec. III.A and detailed in the Appendix. The error in pixel location for each grid point was about 0.34 pixels. Although the camera calibration model used here has been shown to give an accuracy of 1/50th of a pixel with computer-generated random noise,[23] errors in locating the markers on the three-dimensional model seem to reduce this accuracy. A 2×2 filter (binning average) was used to reduce the spatial resolution of the PSP image to be comparable to conventional pressure port data (approximately 1 mm). This also helps in attenuating the inherent noise associated with pixel-to-pixel variations in the CCD array and helps to compare with pressure port data.

The image-warping approach uses the polynomial (order 3) transform, which is then ratioed in the normal way. This method was chosen because the polynomial is the commonly used approach in processing PSP data. The ratioed image is then resected onto the grid with the same 2×2 filter as for the direct resection approach. Figure 6 shows the C_p on the surface grid obtained by the direct resectioning of each image onto the surface grid, followed by ratioing. The x and y coordinates have been normalized by the length of the model. The pressure ports (image diameter: two pixels) on the model are visible in the ratioed image. This implies that the resection of each image onto the grid has been accomplished with an error lesser than two pixels. This illustrates the accuracy of the data. Comparisons of the data with pressure port measurements made in the following paragraphs will prove this point. However, the resection-before-ratio approach is computationally more intensive. The computation time per image was about 8 s/image on a P4 at 1.8 GHz with 1 GB of RAM as compared to 3 s/image for producing the field image by the polynomial (order 3) method. The total time was hence 32 and 17 s (3 s/image $\times$ 3 images + resectioning of field image on to grid) for the resection and polynomial approaches respectively.

Figure 7, which is the resection of the image warped and ratioed field image (which is also Fig. 5c) onto the surface grid, illustrates the lesser accuracy of the polynomial approach. Here, in contrast to Fig. 6, we see that the pressure ports and markers are not clearly

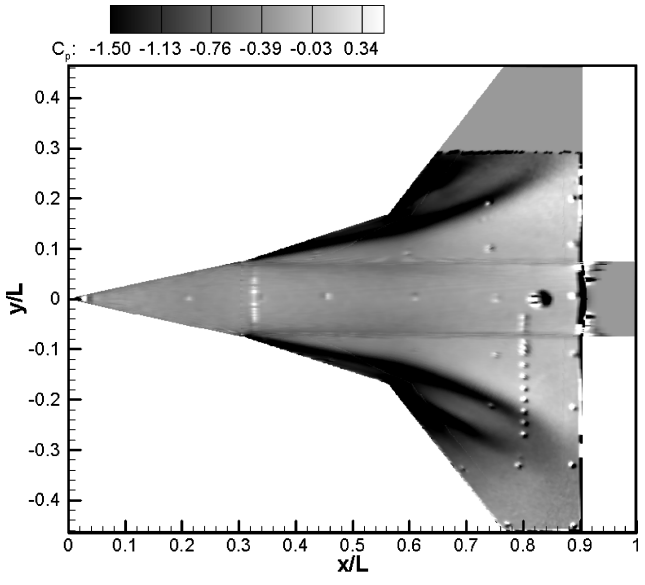

Fig. 6 C_p on surface grid using resection method.

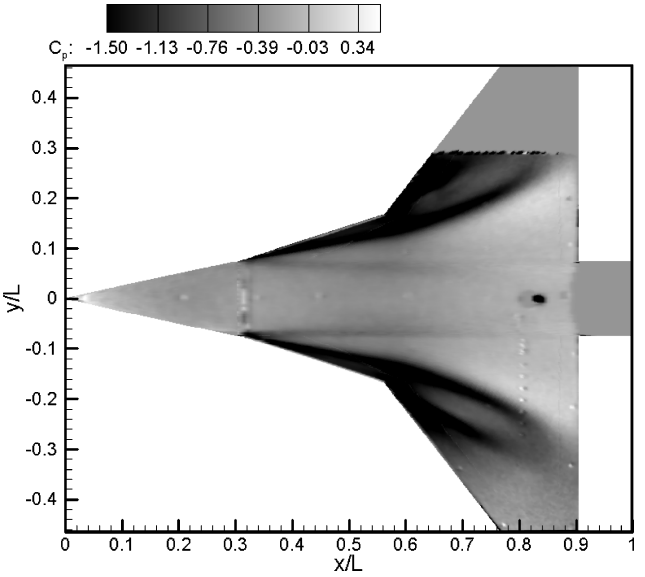

Fig. 7 C_p on surface grid using polynomial transformation followed by resection.

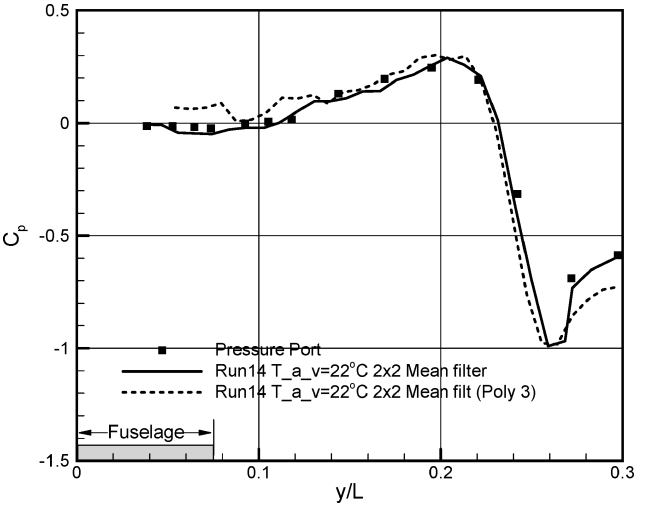

Fig. 8 Comparison of mean pressure at a section from PSP methods and pressure ports.

visible, despite the same resection process used to map the ratioed image on to the surface grid. The third-order polynomial used has a smoothing effect, and the subsequent filtering has erased out the markers and pressure ports.

Figure 8 shows a comparison with pressure port data with the two approaches. The data shown are for half the fuselage and the wing containing the pressure ports. The uncertainty of the pressure port measurements is within $\pm 0.02 C_p$ (Ref. 27), which is about the size of the symbol in the figure. Both approaches appear to yield similar accuracies and show agreement with the port data, though the resection prior to ratioing (second approach) gives better results over the body and towards the wing tip and also on the fuselage section. Further, the PSP data in both cases indicate a minimum C_p lower than that captured by the ports; the results suggest that the minimum occurs between two ports and a larger number of pressure ports on the model would have captured the same more accurately. The rms deviations from the pressure port data are 0.0939 and 0. 0353 in C_p for the polynomial and resection approaches, respectively.

For the freestream Mach number and incidence chosen here, the streamwise pressure gradients are relatively low in the region of the pressure ports, and hence, the two approaches seem to yield comparable accuracy. Figure 9 compares data from the two approaches at an axial station across the entire image (both wings and fuselage)

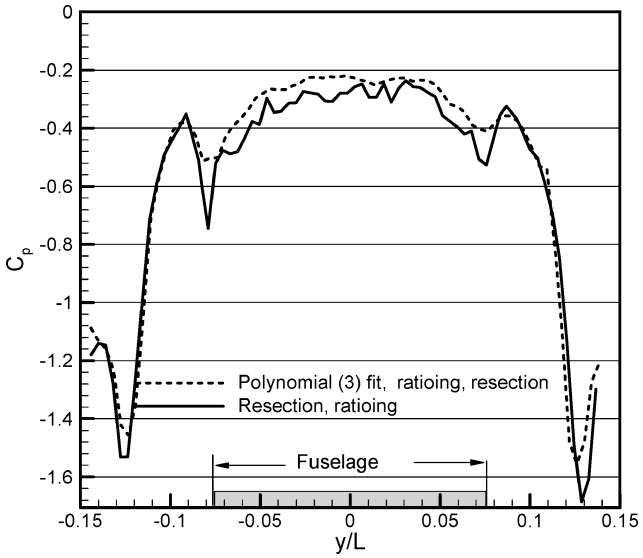

Fig. 9 Comparison of mean pressure near leading edge of wing from the two PSP approaches.

of $x/L = 0.35$, which is near the leading edge of the wing. Here the differences in the resolution of the two methods are clearly visible. The minimum C_p obtained for the direct resection case is lower than for the resected polynomial case. The wing-body intersection is clearly picked up in the former case. This is caused by the smoothing effect of the image registration step using the polynomial approach. Although there are no pressure ports at this station for comparison, this conclusion is supported by the fact that the resection approach provides better spatial resolution.

VI. Conclusions

This paper has attempted a systematic comparison of the two well-known approaches of image registration, namely, image warping and resection. PSP test data obtained on a generic wing-body model at a freestream M of 0.6 and incidence of 10 deg (taken from earlier work) along with conventional static port data are utilized to assess critically the accuracy of the two approaches. A comprehensive camera model, which takes into account the lens distortions as well as errors in identifying marker locations, is used to resect each of the wind-on and wind-off images from both cameras onto a three-dimensional body surface grid, prior to ratioing. This is compared with image warping employing a third-order polynomial transform and ratioing prior to resecting the ratio onto the surface grid, using the same camera model.

A comparison of different image warping methods has shown that the misalignment on a wing-body combination varies from 3 to 35 pixels depending on the surface and the method used. The largest misalignment was generally observed on the fuselage. The error in alignment using a third-order polynomial method was found to be around five and 15 pixels on the wings and fuselage, respectively, whereas for the resection before ratioing approach, it was less than a pixel everywhere on the model. The resection approach yields much higher resolution in regions having large pressure gradients or on bodies that are significantly three dimensional and is to be preferred, despite slightly larger computing time. Although the comparison was carried out for a two-camera system (binary luminophore), even a single-camera system (single luminophore) undergoing rigid-body rotation or translation under wind loads could be a suitable candidate for the resection approach.

The successful application and favorable results from the resection approach promise improved applicability of pressure-sensitive paint to complex configurations and accuracy comparable to conventional pressure measurements.

Appendix: Camera Model

Figure 2 shows a pure-perspective-projection (pinhole camera) camera model.[23] The lens of the camera is modeled by a single point called perspective center (X_c, Y_c, Z_c), which is also the origin of the image coordinate system (center of projection O) in model coordinate space.

The image plane is parallel to XY plane and at a distance f (focal length) along the z axis. The orientation of the image coordinate system with respect to the model system is given by a 3×3 rotation matrix R, whose nine terms are not independent and can be reduced to three parameters by taking the Euler-angle approach. This implies that R is a calculation of three separate rotations about three principal axes. If the rotations about X, Y, Z are denoted by ω, ϕ, and κ, then

$$R = R_z(\kappa)R_y(\phi)R_x(\omega), \qquad R_x(\omega) = \begin{bmatrix} 1 & 0 & 0 \\ 0 & \cos\omega & -\sin\omega \\ 0 & \sin\omega & \cos\omega \end{bmatrix}$$

$$R_y(\phi) = \begin{bmatrix} \cos\phi & 0 & \sin\phi \\ 0 & 1 & 0 \\ -\sin\phi & 0 & \cos\phi \end{bmatrix}$$

$$R_z(\kappa) = \begin{bmatrix} \cos\kappa & -\sin\kappa & 0 \\ \sin\kappa & \cos\kappa & 0 \\ 0 & 0 & 1 \end{bmatrix} \tag{A1}$$

We note that the rotations are not commutative:

$$R = \begin{bmatrix} \cos\phi\cos\kappa & -\cos\omega\sin\kappa + \sin\omega\sin\phi\cos\kappa & \sin\omega\sin\kappa + \cos\omega\sin\phi\cos\kappa \\ \cos\phi\sin\kappa & \cos\omega\cos\kappa + \sin\omega\sin\phi\sin\kappa & -\sin\omega\cos\kappa + \cos\omega\sin\phi\sin\kappa \\ \sin\phi & \sin\omega\cos\phi & \cos\omega\cos\phi \end{bmatrix} \tag{A2}$$

Consider a point XYZ in model space. For an ideal camera the projection is at (x, y), but because of distortion the image of the point is at (x', y'). The relation between image and model coordinates is expressed via the projective equation of photogrammetry, also known as the collinearity equations[24]:

$$x - x_p = x' - x_p + \Delta x = -f\frac{r_{11}(X - X_c) + r_{12}(Y - Y_c) + r_{13}(Z - Z_c)}{r_{31}(X - X_c) + r_{32}(Y - Y_c) + r_{33}(Z - Z_c)}$$

$$y - y_p = y' - y_p + \Delta y = -f\frac{r_{21}(X - X_c) + r_{22}(Y - Y_c) + r_{23}(Z - Z_c)}{r_{31}(X - X_c) + r_{32}(Y - Y_c) + r_{33}(Z - Z_c)} \tag{A3}$$

where X_c, Y_c, Z_c is the origin of the camera frame, also known as perspective center; f is the focal length of the lens, also known as principal distance (the distance of the image plane from the perspective center parallel to z axis); and x_p, y_p is the principal point, which is the intersection of the perpendicular from perspective center to image plane and subscripts r_{ij} are the elements of the rotation matrix R. Δx and Δy are the terms that model the effects of symmetric and

asymmetric lens distortion. This is because in real cameras perspective projection is not sufficient for modeling the mapping precisely. Ideally, the object point, perspective center, and image point lie along a straight line. However, in practice lens systems are composed of several optical elements introducing nonlinear distortion to optical path and resulting images.

The lens distortion terms can be modeled as the sum of radial distortion and decentering distortion[25]:

$$\mathrm{d}x = \mathrm{d}x_r + \mathrm{d}x_d, \qquad \mathrm{d}y = \mathrm{d}y_r + \mathrm{d}y_d$$

$$\mathrm{d}x_r = k_1(x' - x_p)r^2 + k_2(x' - x_p)r^4 - k_3(x' - x_p)r^6$$

$$\mathrm{d}y_r = k_1(y' - y_p)r^2 + k_2(y' - y_p)r^4 - k_3(y' - y_p)r^6$$

$$\mathrm{d}x_d = P_1\left[r^2 + 2(x' - x_p)^2\right] + 2P_2(x' - x_p)(y' - y_p)$$

$$\mathrm{d}y_d = P_1\left[r^2 + 2(y' - y_p)^2\right] + 2P_1(x' - x_p)(y' - y_p)$$

$$r = \sqrt{(x' - x_p)^2 + (y' - y_p)^2} \tag{A4}$$

where k_1, k_2, k_3 are the radial distortion coefficients that cause the image point to be displaced radially in the image plane and P_1, P_2 are coefficients for decentering and tangential distortion that occur if the centers of curvatures of the lens systems are not strictly collinear. The affinity distortion parameters that are used if the image axes are not orthogonal have been neglected as most CCD arrays are almost perfect rectangles and the distortion component is less than 0.01 pixels.[26]

The parameters $(X_c, Y_c, Z_c, \omega, \phi, \kappa)$ are called the extrinsic or exterior projective parameters, and $(k_1, k_2, k_3, P_1, P_2, x_p, y_p, f)$ are called intrinsic or internal projective parameters.

If the number of markers in the model is m, the camera images m points; the total number of unknowns are $6n + 8$ (where n is number of camera locations, here single; eight is the number of internal parameters). This results in 2 m number of equations; hence, a minimum of seven marker points is needed at each camera location. The system is usually overdetermined and is hence solved in a least-squares sense. We thus need to first correct for the distortion and then estimate the camera parameters. However, the distortion coefficients are not usually known in advance and because of strong coupling cannot be reliably estimated without knowing the other camera parameters. This results in a nearly singular normal equation matrix of the least-squares problem.

A commonly used approach in photogrammetry[25] to avoid the singularity is to use the least-squares estimation for only the external parameters, while the interior orientation and lens distortion parameters are calculated separately using an optimization method. For the initial guess, the direct linear transform (DLT)[21] is used:

$$x = \frac{L_1X + L_2Y + L_3Z + L_4}{L_9X + L_{10}Y + L_{11}Z}, \qquad y = \frac{L_5X + L_6Y + L_7Z + L_8}{L_9X + L_{10}Y + L_{11}Z} \tag{A5}$$

where $L1 \ldots L11$ are called the DLT coefficients and are related to the external and internal parameters. This ignores Δx and Δy and gives poor estimates of the principal point (x_p, y_p), but it can provide an initial estimate to the optimization method. Heikkilä[23] points out that the major shortcoming is that it is not an optimal estimator, as it does not produce minimum variance estimates and thus rather sensitive to observation noise. He concludes that for the initialization step it is more reliable to use the nominal values for the focal length, aspect ratio, and image center as the intrinsic parameters.

The solution in the least-squares sense is obtained by first recasting the equations in a convenient form.[13] Let $\boldsymbol{\xi}$ be a vector of unknowns:

$$\boldsymbol{\xi} = \xi(\chi_c, \Phi, \Psi)^T \tag{A6}$$

where $\chi_c \equiv (X_c, Y_c, Z_c)$, $\Phi \equiv (\omega, \phi, \kappa)$ are the camera external parameters and $\boldsymbol{\Psi} \equiv (k_1, k_2, k_3, P_1, P_2, x_p, y_p, f)$ is the vector of the camera internal parameters. Then we can rewrite the equations as[13]

$$\mathbb{F}(\xi) = \begin{bmatrix} F_l(\xi) = (x'_j + \Delta x_j - x_p)(\chi_j - \chi_c) \cdot \hat{r}_3 + f(\chi_j - \chi_c) \cdot \hat{r}_1 = 0 \\ G_l(\xi) = (y'_j + \Delta y_j - y_p)(\chi_j - \chi_c) \cdot \hat{r}_3 + f(\chi_j - \chi_c) \cdot \hat{r}_1 = 0 \end{bmatrix} \tag{A7}$$

where $\boldsymbol{\chi}_j \equiv (X_j, Y_j, Z_j)$ is the position vector of the jth target, $\boldsymbol{\chi}_c$ is the position vector of the camera, and $\hat{r}_k$ is the unit vector corresponding to the kth column of R and a function of the camera angles (ω, ϕ, κ). This is solved in an iterative fashion. Assume ξ is known at iteration k. The left-hand side of the preceding equation can be expressed as a truncated Taylor series at iteration $k + 1$:

$$\mathbb{F}^{k+1}(\xi) = \mathbb{F}^k(\xi) + \left(\frac{\partial \mathbb{F}}{\partial \xi}\right)\boldsymbol{\Delta\xi}^k \tag{A8}$$

where $\boldsymbol{\Delta\xi}^k = \xi^{k+1} - \xi^k$, $\mathbb{F}$ is a column vector with $2m$ elements, the Jacobian $\partial\mathbb{F}/\partial\xi$ is a matrix with $2m$ rows and $6n + 8 (= 14)$ columns, and $\boldsymbol{\Delta\xi}$ is a column vector with 14 elements.

Solving for ξ^{k+1} using Newton–Raphson iteration, we get

$$\xi^{k+1} = \xi^k - \left[\left(\frac{\partial \mathbb{F}}{\partial \xi}\right)^k\right]^{-1} \mathbb{F}^k(\xi) \tag{A9}$$

where $[(\partial\mathbb{F}/\partial\xi)^k]^{-1}$ is the pseudoinverse of the Jacobian. The elements of the Jacobian can be determined analytically in the manner detailed by Samtaney.[13] The solution is iterative, solving a system of linear equations at each step. As pointed out already, in most cases the system is overdetermined, and the solution is in least-squares sense. The convergence criterion $|\mathbb{F}^{k+1} - \mathbb{F}^k| = \varepsilon$, where ε is a "small enough" number (here chosen as 10^{-4}), is used.

Acknowledgments

The author thanks Channa Raju for use of the pressure-sensitive-paint (PSP) data and extensive discussions on PSP data processing and P. R. Viswanath, Head, Experimental Aerodynamics Division, for many insightful discussions and encouragement. J. S. Mathur of CTFD generated the GRIDGEN surface grid on the model. Mahesh Kadam obtained the marker coordinates using the coordinate measuring machine.

References

[1]Bell, J. H., Schairer, E. T., Hand, L. A., and Mehta, R. D., "Surface Pressure Measurements Using Luminescent Coatings," *Annual Review of Fluid Mechanics*, Vol. 33, 2001, pp. 155–206.

[2]Bell, J. H., and McLachlan, B. G., "Image Registration for Luminescent Paint Sensors," AIAA Paper 93-0178, Jan. 1993.

[3]Bell, J. H., and McLachlan, B. G., "Image Registration for Pressure-Sensitive Paint Applications," *Experiments in Fluids*, Vol. 22, No. 1, 1996, pp. 78–86.

[4]Sullivan, J., "Temperature and Pressure Sensitive Paint," *Advanced Measurement Techniques*, edited by C. H. Sleverding, Lecture Series 2000–2001, von Kármán Inst. for Fluid Mechanics, Brussels, 2001.

[5]Buck, G. M., "Simultaneous Global Pressure and Temperature Measurements Technique for Hypersonic Wind Tunnels," AIAA Paper 2000-2646, June 2000.

[6]LeSant, Y., Deliglise, B., and Mebarki, Y., "An Automatic Image Alignment Method Applied to Pressure Sensitive Paint Measurements," *ICIASF '97 Record*, International Congress on Instrumentation in Aerospace Simulation Facilities, 1997, pp. 94–104.

[7]Liu, T., Cattafesta, L. N., III, Radeztsky, R. H., and Burner, A. W., "Photogrammetry Applied to Wind-Tunnel Testing," *AIAA Journal*, Vol. 38, No. 6, 2000, pp. 964–971.

[8]Ruyten, W., "Towards an Integrated Optical Data System for Wind Tunnel Testing," AIAA Paper 99-0581, Jan. 1999.

[9]Le Sant, Y., and Merienne, M.-C., "An Image Resection Method Applied to Mapping Techniques," *16th International Congress on Instrumentation in Aerospace Simulation Facilities*, 95CH3482-7, Inst. of Electrical and Electronics Engineers, 1995, pp. 46.1–46.8.

[10]Weaver, W. L., Jordan, J. D., Dale, G. A., and Navarra, K. R., "Data Analysis for the Development and Deployment of Pressure Sensitive Paints," AIAA Paper 99-0565, 1999.

[11]Park, S. H., and Sung, H. J., "Correlation-Based Image Registration for Applications Using Pressure-Sensitive Paint," *AIAA Journal* (to be published); also AIAA Paper 2004-0882, Jan. 2004.

[12]Donovan, J., Morris, M., Pal, A., Benne, M., and Crites, R., "Data Analysis Techniques for Pressure and Temperature-Sensitive Paint," AIAA Paper 93-0176, Jan. 1993.

[13]Samtaney, R., "A Method to Solve Interior and Exterior Camera Calibration Parameters for Image Resection," NASA TR 99-003, April 1999.

[14]Fonov, S., Crafton, J., Goss, L., Jones, G., and Fonov, V., "Near-Real-Time Pressure Field Visualization," *19th International Congress on Instrumentation in Aerospace Simulation Facilities, ICIASF '01*, Inst. of Electrical and Electronics Engineers, 2001.

[15]Ruyten, W., "More Photogrammetry for Wind-Tunnel Testing," *AIAA Journal*, Vol. 40, No. 6, 2002, pp. 1277–1283.

[16]Ruyten, W., and Sellers, L., "On-Line Processing of Pressure-Sensitive Paint Images," AIAA Paper 2003-3947, June 2003.

[17]Novak, K., "Rectification of Digital Imagery," *Photgrammetric Engineering and Remote Sensing*, Vol. 58, No. 3, 1992, pp. 339–344.

[18]Jain, A., *Fundamentals of Digital Image Processing*, Prentice–Hall, Upper Saddle River, NJ, 1986, pp. 321, 322.

[19]Atkinson, K. B. (ed.), *Close Range Photogrammetry and Machine Vision*, Whittles Publishing, Caithness, Scotland, U.K., 1996.

[20]Devereux, B., Fuller, R., Carter, L., and Parsell, R., "Geometric Correction of Airborne Scanner Imagery by Matching Delaunay Triangles," *International Journal of Remote Sensing*, Vol. 11, No. 12, 1990, pp. 2237–2251.

[21]Shanmugasundaram, R., and Samareh-Abolhossani, J., "Modified Scatter Data Interpolation Used to Correct Pressure Sensitive Paint Images," AIAA Paper 95-2041, June 1995.

[22]Goshtasby, A., "Image Registration by Local Approximation Methods," *Image and Vision Computing*, Vol. 6, No. 4, 1988, pp. 255–261.

[23]Heikkilä, J., "Geometric Camera Calibration Using Circular Control Points," *IEEE Transactions Pattern Analysis and Machine Intelligence*, Vol. 22, No. 10, 2000, pp. 1066–1077.

[24]Slama, C., *Manual of Photogrammetry*, 4th ed., American Society of Photogrammetry, Falls Church, VA, 1980.

[25]Abdel-Aziz, Y., and Karara, H., "Direct Linear Transformation from Comparator Coordinates into Object Space Coordinates," *Proceedings of the Symposium on Close-Range Photogrammetry*, American Society of Photogrammetry, Falls Church, VA, 1971, pp. 1–18.

[26]Venkatakrishnan, L., "Application of Resection to PSP Image Registration," National Aerospace Labs., NAL PD EA 0314, Bangalore, India, Nov. 2003.

[27]Channa Raju and Viswanath, P. R., "Pressure Sensitive PAINT Measurements in NAL 1.2m Blowdown Wind Tunnel," National Aerospace Labs., NAL PD 0313, Bangalore, India, Nov. 2003.

R. Lucht
Associate Editor